

Implications of the *Fermi*-LAT Pass 8 Galactic Center Excess on Supersymmetric Dark Matter

Abraham Achterberg^a Melissa van Beekveld^a Sascha Caron^{a,b}
Germán A. Gómez-Vargas^c Luc Hendriks^a Roberto Ruiz de
Austri^d

^aInstitute for Mathematics, Astrophysics and Particle Physics, Faculty of Science, Mailbox 79, Radboud University Nijmegen, P.O. Box 9010, NL-6500 GL Nijmegen, The Netherlands

^bNikhef, Science Park, Amsterdam, The Netherlands

^cInstituto de Astrofísica, Pontificia Universidad Católica de Chile, Avenida Vicuña Mackenna 4860, Santiago, Chile

^dInstituto de Física Corpuscular, IFIC-UV/CSIC, Valencia, Spain

E-mail: a.achterberg@astro.ru.nl, mcbeekveld@gmail.com, scaron@cern.ch,
ggomezv@uc.cl, luc@luchendriks.com, rruiz@ific.uv.es

Abstract. The *Fermi* Collaboration has recently updated their analysis of gamma rays from the center of the Galaxy. They reconfirm the presence of an unexplained emission feature which is most prominent in the region of 1 – 10 GeV, known as the Galactic Center GeV excess (GCE). Although the GCE is now firmly detected, an interpretation of this emission as a signal of self-annihilating dark matter (DM) particles is not unambiguously possible due to systematic effects in the gamma-ray modeling estimated in the Galactic Plane. In this paper we build a covariance matrix, collecting different systematic uncertainties investigated in the *Fermi* Collaboration’s paper that affect the GCE spectrum. We show that models where part of the GCE is due to annihilating DM is still consistent with the new data. We also re-evaluate the parameter space regions of the minimal supersymmetric Standard Model (MSSM) that can contribute dominantly to the GCE via neutralino DM annihilation. All recent constraints from DM direct detection experiments such as PICO, LUX, PandaX and Xenon1T, limits on the annihilation cross section from dwarf spheroidal galaxies and the Large Hadron Collider limits are considered in this analysis. Due to a slight shift in the energy spectrum of the GC excess with respect to the previous *Fermi* analysis, and the recent limits from direct detection experiments, we find a slightly shifted parameter region of the MSSM, compared to our previous analysis, that is consistent with the GCE. Neutralinos with a mass between 85 – 220 GeV can describe the excess via annihilation into a pair of *W*-bosons or top quarks. Remarkably, there are models with low fine-tuning among the regions that we have found. The complete set of solutions will be probed by upcoming direct detection experiments and with dedicated searches in the upcoming data of the Large Hadron Collider.

Contents

1	Introduction	2
2	The Galactic Center Excess	5
3	Models and Constraints	9
4	Results	11
5	Conclusion	18

1 Introduction

There is overwhelming evidence that the matter content of the Universe mostly consists of dark matter (DM). What still remains unknown is its nature, that is, whether it is a fundamental particle and how it interacts with the Standard Model (SM) of fundamental interactions. There are many extensions of the SM that predict particles that could account for the DM we observe. Among them, the so-called weakly interactive massive particles (WIMPs) are the more popular ones. WIMPs naturally achieve the required relic density through self-annihilation in the early Universe [1]. Precisely this self-annihilation mechanism would allow indirect DM detection in the present Universe by observing the stable annihilation products, such as gamma rays. In our galaxy this predicted gamma radiation could be detected by the Large Area telescope (LAT), on board the *Fermi* Gamma-ray Space Telescope [2].

The Galactic Center Excess (GCE) is a feature in the gamma-ray data collected from the Inner Galaxy with the *Fermi*-LAT. The dominant contribution of the total emission detected can be explained using Interstellar Emission Models (IEMs) tuned with Galactic plane data and point source catalogs. The GCE is a sub-dominant component ($\sim 10\%$) of the observed flux. The spectral energy distribution of the GCE peaks at about 3 GeV [3–12]. Among different IEMs and source lists, the GCE is well described spatially with a generalized Navarro, Frenk and White (NFW) dark matter density profile [13, 14] with reduced inner slope (index 1.25).

Two *Fermi*-LAT Collaboration papers have confirmed the GCE [15, 16]. In particular, the latest work presents an updated status of the GCE using the reprocessed Pass 8 event data collected in about 6.5 years of observations¹ [16]. A large set of systematic sources of uncertainty in the extraction of the GCE properties (spectral shape, magnitude and morphology) were investigated in ref. [16]. This results in an excess spectrum that is most prominent in the photon energy range of 1-10 GeV and has a smaller high energy tail starting at photon energies of 10 GeV. The spatial morphology of the GCE in these two energy ranges seem to be different from one another, the first energy range being compatible with a DM signal and at energies larger than about 10 GeV with an X-shaped morphology is instead observed [16]. One concludes that the GCE is detected but that, given the magnitude of systematic uncertainties, a firm interpretation of the excess as a signal from DM annihilation is not possible, but also not excluded.

A possible interpretation of the GCE comes from the fact that 205 pulsars have been identified in the gamma-ray band². A population of pulsars is expected in the Galactic bulge [17]. Based on these assumptions many previous studies have investigated the possibility that a population of unresolved gamma-ray pulsars could be the reason of the GCE emission [18–23]. For instance, ref. [23] concludes that about 60 Galactic bulge pulsars should have been already seen by the *Fermi*-LAT, but have not been identified as pulsars. Furthermore, using novel statistical methods, the authors of ref. [24] and ref. [25] have claimed evidence for the existence of an unresolved population of gamma-ray sources in the inner 20 deg of the Galaxy, with a spatial distribution and collective flux compatible with the GCE.

Recently the *Fermi*-LAT Collaboration investigated the pulsar interpretation of the GCE [16]. Performing a new point source search in 7.5 years of Pass 8 *Fermi*-LAT data in a $40^\circ \times 40^\circ$ box around the GC, they claim to confirm the findings of ref. [24] and ref. [25]. In this analysis they detect 400 sources, with 66 of them being gamma-ray pulsar candidates.

¹The data of the analysis in [16] is publicly released here https://www-glast.stanford.edu/pub_data/1220/

²See <https://confluence.slac.stanford.edu/x/5Jl6Bg> for the list of detected γ -ray point pulsars.

They also find that these sources are more likely to be the brighter members of a larger underlying population of pulsars in the Galactic bulge rather than Galactic bar pulsars. They find that the collective emission of gamma-ray pulsars in the bulge population is compatible with the GCE properties. However, some arguments [26–28] have been raised against this explanation, pointing out that a gamma-ray millisecond pulsar (MSP) population in the Galactic bulge with similar properties of already confirmed populations in globular clusters³ and the local Galactic disc⁴, is not able to reproduce the whole GCE emission. The weak point of those arguments is the assumption that a MSP population in the Galactic bulge shares similarities with populations in different environments and with a diverse origin, such as in globular clusters and the local Galactic disc [29]. Therefore the debate is not yet closed, leaving the possibility that the entire GCE or a fraction of the GCE is due to DM (WIMP) annihilation. Therefore, new methods are needed to analyze γ -ray data (see [30]) to detect the pulsar population at other wavelengths and to determine the true nature of the excess. There have been many attempts in the literature to fit the GCE through WIMPs, mainly using simplified models. These simplified models do not cover the full phenomenology of more complete and more complex models, e.g. the only possible signature at the LHC could come from the production of a particle which is not present in the simplified model. Therefore Supersymmetry (SUSY) in its minimal phenomenological realization, the so called phenomenological Minimal Supersymmetric Standard Model (pMSSM) [31], has also been investigated in ref. [32–39]. Those analyses found that two regions at a DM mass around ≈ 85 GeV and ≈ 180 GeV are compatible with the excess. In this case, DM is the lightest neutralino⁵ and is a mixture which is dominantly bino and has subdominant wino and/or higgsino components.

The pMSSM parameter regions consistent with the GCE lead to novel DM signals at the Large Hadron Collider (LHC), not covered by searches for simplified models or other SUSY scenarios [40]. Interestingly one of the higgsino-bino regions is consistent with one of the lowest fine-tuning values of the electroweak sectors found in the pMSSM[41].

In this work we revisit the GCE interpretation in terms of the pMSSM through a fit to the new *Fermi*-LAT data, accounting for the most up-to-date phenomenological constraints. In particular we consider the constraints from direct DM searches in experiments like LUX [42], PANDAS [43], XENON1T [44] and PICO [45], as well as from SUSY searches at the LHC. The solutions that we find explain the GCE in the photon energy range from 1 to 10 GeV. To account for the high-energy tail of the GCE, we assume an universal power law as different phenomena have been proposed to explain it based on its tentative X-shaped morphology [46–48]. We will give no further astrophysical interpretation of the high energy tail.

The paper is organized as follows: in section 2 we describe the status of the GCE as revealed with Pass 8 data, while in Section 3 we describe the details of the present analysis. In section 4 we show the results and discuss the prospects of the pMSSM scenario in terms of

³For instance in ref. [28], assuming that the ratio between low mass x-ray binaries to MSPs in globular clusters is the same as in the bulge, it is shown that the MSP contribution to the GCE emission is limited to 4% to 23%.

⁴The authors of [27] argue that if the luminosity function of local Galactic disc MSPs is assumed for the bulge population, the *Fermi*-LAT should have detected many of its bright members in the GC region, but none have been identified yet.

⁵Neutralinos are fermionic partner particles of the Standard Model bosonic fields (i.e. the B, W and Higgs fields). Corresponding to their composition the neutralinos can be binos (partners of B-field), winos (partners of W fields), higgsinos (Higgs partners) or a combination of these quantum states.

LHC run II and direct dark matter searches. Finally, in Section 5 we discuss the implication of the results and present our conclusions.

2 The Galactic Center Excess

Our analysis uses the GCE measurements presented in ref. [16], whose analysis significantly benefits from Pass 8 event-level data due to its improvement in acceptance, the reconstruction of arrival direction and energy, and the sub-selection of events based on the quality of the direction reconstruction. The GCE spectrum is shown in figure 1. In ref. [16] the following effects of the systematic uncertainties affecting the properties of the GCE were investigated:

1. Changes in the *Fermi*-LAT event selection and analysis region.
2. Using different assumptions for cosmic ray (CR) production and propagation in the Galaxy (GALPROP parameters [49, 50]), and allowing for more freedom in the fit to inverse Compton (IC) emission [51] (both indicated by the gray lines in figure 1).
3. The inclusion of CR sources in the GC region that can induce gamma-ray emission
4. The use of alternative distributions of interstellar gas in the GC region.
5. The extension of the *Fermi* bubbles to the GC with a data driven method designed to quantify its role in the GCE.
6. As the point sources near the GC region strongly depend on the IEM used to describe the diffuse emission, different point source catalogs based on different IEMs and analyses are tested.

In all the scenarios listed above the GCE is found to be statistically significant. However, the GCE spectral shape varies in the scenarios tested in the following way: at photon energies between 1 and 3 GeV, the flux changes by a factor of ~ 3 . Above 10 GeV the change is significantly larger, even compatible with zero flux for some background models (gray lines in figure 1) [16]. In order to consider the systematic uncertainties explored in ref. [16] we create *two covariance matrices* to capture the effects on the GCE due to:

- The excesses found along the Galactic plane, see figure 2a.
- The variations in the GCE due to item 2 listed above⁶, see figure 2b.

To compute the covariance matrices we use (section 4.2.2 of ref. [10]):

$$\Sigma_{i,j} = \langle \Phi_i \Phi_j \rangle - \langle \Phi_i \rangle \langle \Phi_j \rangle. \quad (2.1)$$

Here, Φ_i represents the measured gamma-ray flux at the i -th energy bin (the black points in figure 1). The average is over the different spectra under consideration to build the covariance matrix. To fit a particular model $\Phi^m(\vec{\theta})$ we find the set of $\vec{\theta}$ parameters that minimizes the χ^2 function:

$$\chi^2 = \sum_{i,j} (\Phi_i^d - \Phi_i^m) \hat{\Sigma}_{ij}^{-1} (\Phi_j^d - \Phi_j^m), \quad (2.2)$$

where Φ_i^d represents the GCE flux in energy bin i . The inverse of the covariance matrix is denoted by $\hat{\Sigma}^{-1}$. To test if a model $\Phi^m(\vec{\theta})$ is rejected as an explanation of the data $\{\Phi^d, \hat{\Sigma}\}$

⁶We restrict ourselves to using these GCE spectra as the other possibilities explored in ref. [16] include astrophysical sources that absorb part of the GCE emission. In this work we model the GCE with two different components to account for these effects.

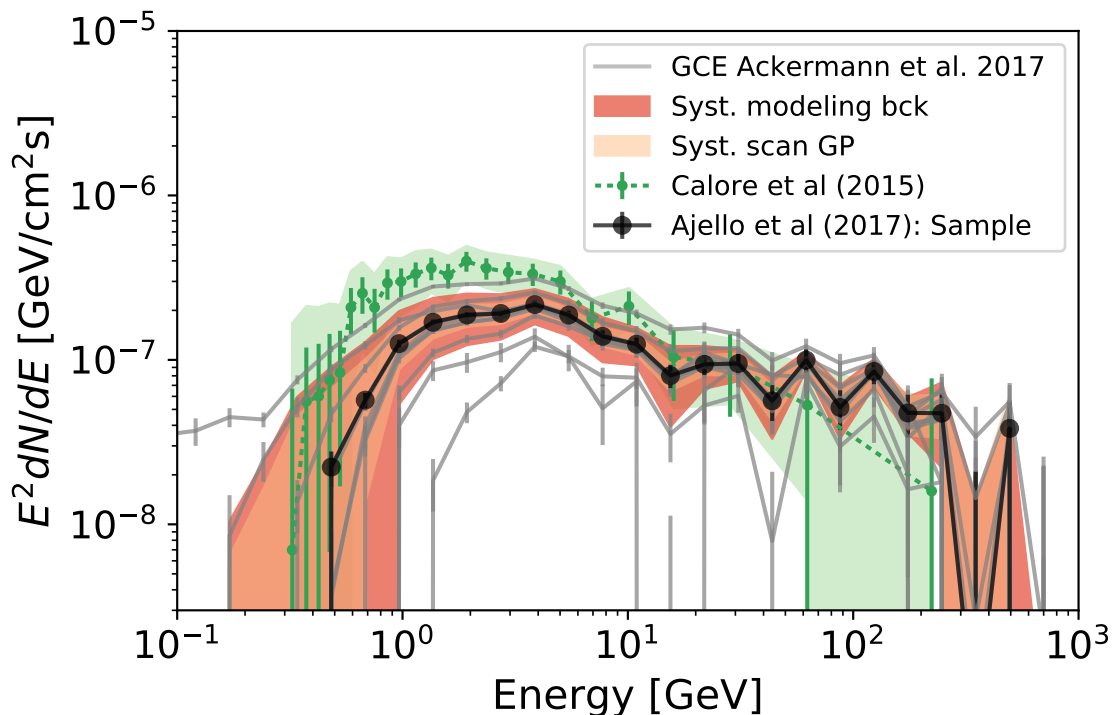


Figure 1: GCE spectra from ref. [16]. Following ref. [16] we select the GCE derived using the Sample Model (see section 2.2 of ref. [16] for description of the model) to perform the fits (black points). The different spectra resulting from using different assumptions for CR production, propagation in the Galaxy and allowing for more freedom in the IC emission fit are shown in gray. The diagonal of two covariance matrices is plotted, one due to excesses found along the Galactic plane in ref. [16] (light orange band), and one due to the set of all GCE spectra plotted in gray (dark orange band). For comparison the GCE spectrum as found in ref. [10] (green points) is plotted together with the diagonal of the covariance matrix derived there (light green band).

we cannot use a reduced χ^2 to compute p-values as the models normally used to fit the GCE are not linear and the data we aim to fit is already obtained from a fit⁷. Therefore we use the following method:

1. Find the set of $\vec{\theta}_{best}$ that minimize χ^2 for a particular $\{\Phi^d, \hat{\Sigma}\}$ and save χ_{best}^2 .
2. Create a set of 100.000 pseudo-random data normal distributed with mean at $\Phi^m(\vec{\theta}_{best})$ according to $\hat{\Sigma}$.
3. Compute χ^2 between $\Phi^m(\vec{\theta}_{best})$ and each one of the 100.000 pseudo-random data created in 2.
4. Create a χ^2 distribution using the values from item 3 and find the values $\chi_{5\%}^2$ and $\chi_{95\%}^2$ at which the integrated distribution covers 5% and 95% of the total χ^2 distribution, respectively.

⁷See ref. [52] for more information.

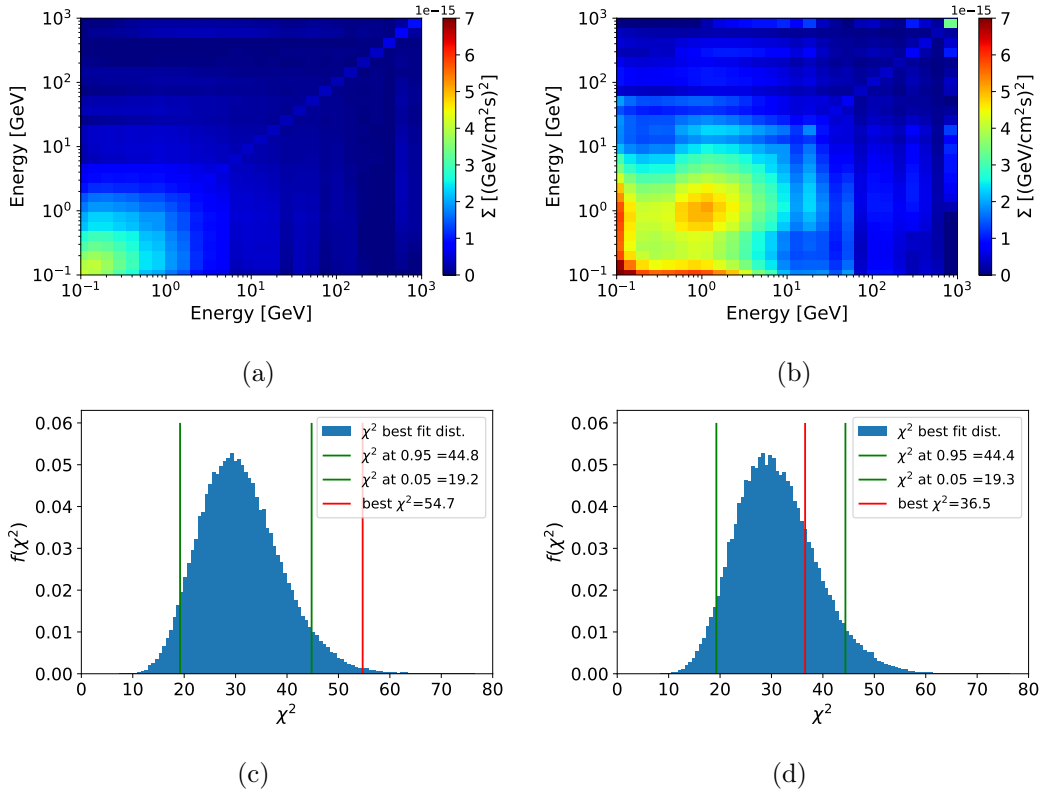


Figure 2: (a) Covariance matrix using statistical uncertainties and the spectra from the analysis along the Galactic plane in ref. [16]. (b) Covariance matrix using the GCE spectra shown by the gray lines in figure 1 plus the statistical uncertainties. (c) Results of scenario 1: the χ^2 distribution of the best fit using the covariance matrix in (a) to fit the toy model of equation 2.3. (d) Results of scenario 2: the χ^2 distribution of the best fit using the composed covariance matrix of (a) and (b) to fit the toy model of equation 2.3.

5. If the χ_{best}^2 found in 1 is lower than $\chi_{5\%}^2$ or greater than $\chi_{95\%}^2$, the $\Phi^m(\vec{\theta}_{best})$ is rejected as an explanation of the data $\{\Phi^d, \hat{\Sigma}\}$ at 95% CL.
6. If the χ_{best}^2 found in 1 is between $\chi_{5\%}^2$ and $\chi_{95\%}^2$, the $\Phi^m(\vec{\theta}_{best})$ *cannot* be rejected as an explanation of the data $\{\Phi^d, \hat{\Sigma}\}$.

In the following we present two examples where we test a toy model to explain the GCE using this method. Our toy model is composed of two power laws with exponential cut-off⁸:

$$\Phi_{toy}^m = \sum_{a=1,2} N_a \left(\frac{E}{E_{0,a}} \right)^{-(\alpha_a - \beta_a \log E/E_{0,a})} e^{-\left(\frac{E - E_{0,a}}{E_{cut,a}} \right)}, \quad (2.3)$$

with N_a two normalizations at reference energies $E_{0,a}$ and with $E_{cut,a}$ the energies of the cut offs.

Scenario 1. Covariance matrix from GP spectra.

First we apply the method using the covariance matrix visualized by figure 2a, where only

⁸A power law with an exponential cut-off is a typical form for the flux originating from astrophysical sources.

the excesses along the Galactic plane plus the statistical uncertainties are considered. The results are presented in figure 2c, where the χ_{best}^2 found tells us that the toy model is rejected as an explanation of the GCE. We expected this result as the toy model looks similar to the DM emission plus *Fermi*-bubbles component tested in ref. [16] and, as already mentioned, that model is found to provide a poor fit to the GCE when considering the excesses along the Galactic plane.

Scenario 2. Covariance matrix considering the GCE spectral variations⁹.

For the second example we apply the method to the same toy model, but instead use a covariance matrix composed of the statistical uncertainties, the systematics associated with the excesses in the Galactic plane (figure 2a) and the variations in the GCE from modeling the Galactic interstellar emission (figure 2b). Results are presented in figure 2d. In this case we find that the toy model can not be rejected as an explanation of the GCE.

Note that in both scenarios, the GCE is significant.

Regarding the DM interpretation of the GCE, the authors of ref. [16] conclude that the spectrum and morphology of the GCE are not evidently consistent with expectations from DM annihilation as DM-like signals observed in other regions of the Galactic plane, where such signals are not expected, give a handle on the magnitude of systematic uncertainties due to diffuse emission modeling in the Galactic Center. However, as discussed in ref. [16], one can not exclude the possibility that the GCE is the result of other gamma-ray sources: for instance a known astrophysical emitter (e.g. Fermi bubbles, millisecond pulsars) on top of a DM-induced component. To explore this possibility we model the GCE spectrum with a component from WIMP annihilation together with a generic astrophysical component. The astrophysical component is modeled as a power law in photon energy with an exponential cut off, like the one shown in equation 2.3. The other power law in the toy model is replaced by SUSY WIMP predictions. We will follow the same procedure to model the uncertainties as in scenario 2. In addition to the uncertainties of the *Fermi*-LAT, we add 10% uncorrelated uncertainty to account for uncertainties in the Monte Carlo event generators that stem from parton showering models and its model parameters [36]. This is achieved by substituting $\hat{\Sigma}_{ij}^{-1} \rightarrow \hat{\Sigma}_{ij}^{-1} + \delta_{ij} (\Phi_i^n)^2 \sigma^2$, where $\sigma = 10\%$ [32]. This will be referred to as the 100% flux scenario.

As was pointed out in section 1, point sources are likely to account for a significant fraction of the GCE. However, sources too dim to be detected individually collectively produce diffuse emission. To take this effect into account, we also explore a hybrid model. Here we assume that gamma-ray emitters of astrophysical origin reduce the GCE flux to 40% of the total flux while keeping the shape intact. The remaining 40% of the total flux is fitted by dark matter annihilation and the one free power law as in the 100% flux scenario. In this hybrid model the uncertainties are downscaled to 40% as well. This will be referred to as the 40% flux scenario.

We have chosen the value of 40%, since the no-DM-hypothesis in this case gives a p-value of 0.056¹⁰. If we reduce the flux even more, the remaining GCE is not significant anymore. The reduced flux shows the effect of the GCE explained by a reduced MSSM DM component on the pMSSM parameter space.

⁹This is the covariance matrix used in this work.

¹⁰The no-DM-hypothesis for the 100% flux scenario amounts to a p-value of 10^{-16} .

3 Models and Constraints

The phenomenological MSSM (pMSSM) [31] is defined by imposing the following constraints on the MSSM:

- One assumes degenerate first and second generation squark and slepton masses.
- All trilinear couplings of the first and second generation sfermions are set to zero.
- There are *no* new sources of CP violation.
- One demands minimal flavor violation, so all sfermion mass matrices are assumed to be diagonal.

Applying these conditions one ends up with a 19-dimensional model that can be parametrized as follows: the sfermion soft-masses are described by the first and second generation squark masses $m_{\tilde{Q}}$, $m_{\tilde{U}_1}$ and $m_{\tilde{D}_1}$, the third generation squark masses $m_{\tilde{Q}_3}$, $m_{\tilde{U}_3}$ and $m_{\tilde{D}_3}$, the first and second generation of slepton masses $m_{\tilde{L}}$, $m_{\tilde{E}}$ and the third generation of slepton masses $m_{\tilde{L}_3}$, $m_{\tilde{E}_3}$. The trilinear couplings of the third generation of sfermions $A_{\tilde{t}}$, $A_{\tilde{b}}$ and $A_{\tilde{\tau}}$ are assumed to be non-zero. The Higgs sector is described by the ratio of the Higgs vacuum expectation values $\tan \beta$ and the soft Higgs masses $m_{H_{u,d}}^2$. Instead of these Higgs masses, we choose to use the higgsino mass parameter μ and the mass of the pseudoscalar Higgs m_A as input parameters. Finally one chooses the gaugino masses M_1 , M_2 and M_3 .

It is nontrivial to scan a large parameter space and apply all constraints stemming from various astrophysical and particle physics experiments [53]. In this paper we use the following strategy. We use the fit points of ref. [32] and ref. [41] as seeds to calculate around 4 million new parameter set evaluations (points). In an iterative procedure the best-fit points of the foregoing iteration are used as additional seeds to sample new model points, where a truncated multi-dimensional Gaussian distribution is used around each parameter of the seed to sample new points [54]. The width of the Gaussian distribution is chosen to be 0.5 times the value of the seed point in each dimension.

SUSPECT [55] is used as spectrum generator, while the Higgs mass is calculated using FeynHiggs [56–60]. MicrOMEGAs 4.3.2 [61] is used to compute flavor variables, $g-2$, $\Omega_{\text{DM}} h^2$, the velocity weighted annihilation cross section and the spin-dependent and spin-independent WIMP-nucleon scattering cross sections (σ_{SD} and σ_{SI}). The gamma ray spectrum is computed using DarkSUSY 5.1.3 [62].

We require the value of observables, as calculated for the model parameters, to lie within the 2σ interval around the experimentally obtained value, unless indicated otherwise. The following limits are applied to the model points:

- LEP limits on the masses of the lightest chargino ($m_{\tilde{\chi}_1^\pm} > 103.5$ GeV) and sleptons ($m_{\tilde{l}} > 90$ GeV) [63].
- Constraints on the invisible and total width of the Z -boson, $\Gamma_{Z,\text{inv}} = 499.0 \pm 1.5$ MeV and $\Gamma_Z = 2.4952 \pm 0.0023$ GeV respectively, obtained from Z -pole measurements at LEP [64].
- The LHC measurements of the Higgs boson mass [38, 65]. On top of this we account for a theoretical SUSY uncertainty of 3 GeV, selecting models with a Higgs boson within the mass range of $122 \text{ GeV} \leq m_{h_0} \leq 128 \text{ GeV}$.

- An upper bound of the muon anomalous magnetic dipole moment $\Delta(g-2)_\mu < 40 \times 10^{-10}$, taking into account the fact that the SM prediction lies well outside the experimentally obtained value: $(24.9 \pm 6.3) \times 10^{-10}$ [66].
- Measurements of the B/D -meson branching fractions: $\text{Br}(B_{(s)}^0 \rightarrow \mu^+ \mu^-)$ [67], $\text{Br}(\bar{B} \rightarrow X_s \gamma)$ [68, 69], $\text{Br}(B^+ \rightarrow \tau^+ \nu_\tau)$ [70], $\text{Br}(D_s^+ \rightarrow \mu^+ \nu_\mu)$ [71] and $\text{Br}(D_s^+ \rightarrow \tau^+ \nu_\tau)$ [72].
- Results of (heavy) Higgs searches at LEP, the Tevatron and the LHC as implemented in HiggsBounds 4.3.1 [73].
- A determination of the exclusion of a model point using SUSY-AI (with the 13 TeV center-of-mass option). SUSY-AI is a machine learning tool, trained with ATLAS data, which is able to exclude model points in the pMSSM parameter space based on ATLAS results [74, 75].
- Limits set by ATLAS on stop production in simplified MSSM scenarios using 2016 ATLAS data, which are not yet included into SUSY-AI. Depending on the stop decay, models are excluded if they fall in the excluded region of the neutralino-stop plane for $\tilde{t} \rightarrow Wb\tilde{\chi}_1^0$ [76], $\tilde{t} \rightarrow c\tilde{\chi}_1^0$ [77, 78] and $\tilde{t} \rightarrow \tilde{\chi}_1^+ b$ [79].
- Constraints on the WIMP-nucleus scattering cross section from various detector experiments, using DDCalc [80] with the 2016 results from LUX [42], the 2017 limits from PICO [45], the 2016 limits from PandaX[43] and the recent XENON1T limits [44]. As in ref. [81], we reject models that are excluded by LUX, PICO, PandaX or XENON1T with more than 3σ to account for the form factor and astrophysical uncertainties. In the regions found in this analysis the limits set by PICO are stronger than the limits set by IceCube [82]. Therefore the limits of IceCube are not used in this analysis.
- The uncertainties of the amount of dark matter in the line-of-sight (the J -factor) are as in ref. [83].
- Limits on the velocity weighted annihilation cross section obtained by analyzing dwarf galaxies [84–86], if the dominant annihilation channel is mainly W^+W^- .

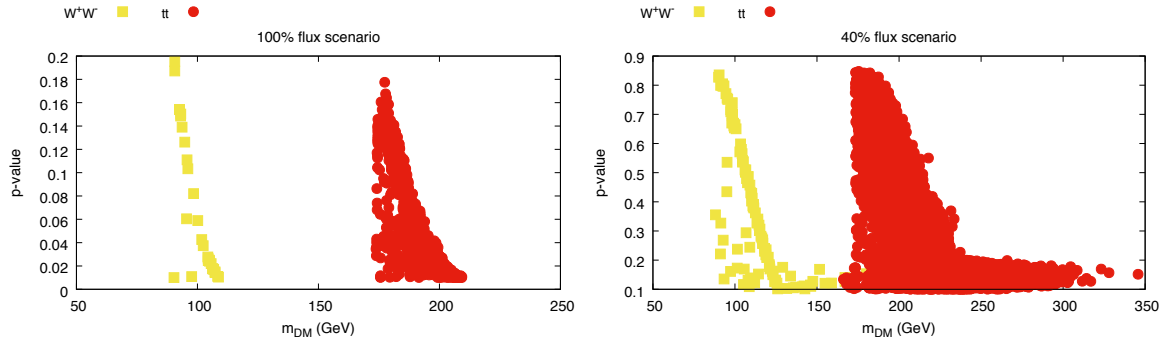


Figure 3: P-value as a function of the dark matter mass for the 100% DM assumption (left figure) and the 40% DM assumption (right figure).

4 Results

Figure 3 shows the p-value of the fit as a function of the DM particle ($\tilde{\chi}_1^0$). Two solutions are visible. For a DM mass between 80 – 120 GeV, DM annihilates predominantly to a pair of W bosons (W^+W^- region). Here the best p-value is 0.19 for the 100% flux scenario and 0.83 for the 40% flux scenario. If the neutralino mass is heavier, the photon spectrum is shifted to higher energies and the fit to the GC excess is worse, as clearly visible in the figure. DM with a mass of 175-220 GeV annihilates predominantly to a pair of top quarks ($t\bar{t}$ region). The best p-value for this region is 0.12 for WW the 100% flux scenario and 0.84 for $t\bar{t}$ the 40% flux scenario. In both cases, the free power law accounts for the tail of the excess, starting at photon energies of 10 GeV. We do not give a further interpretation of the tail of the GCE. We find that, after selecting models that have a Higgs boson in the right mass range and that evade the LEP SUSY mass limit, in particular the dark matter direct detection constraints (both spin-dependent and spin-independent) are important. The other limits listed in section 3, including the limits on the velocity-weighted annihilation cross section, turn out to be of lesser importance.

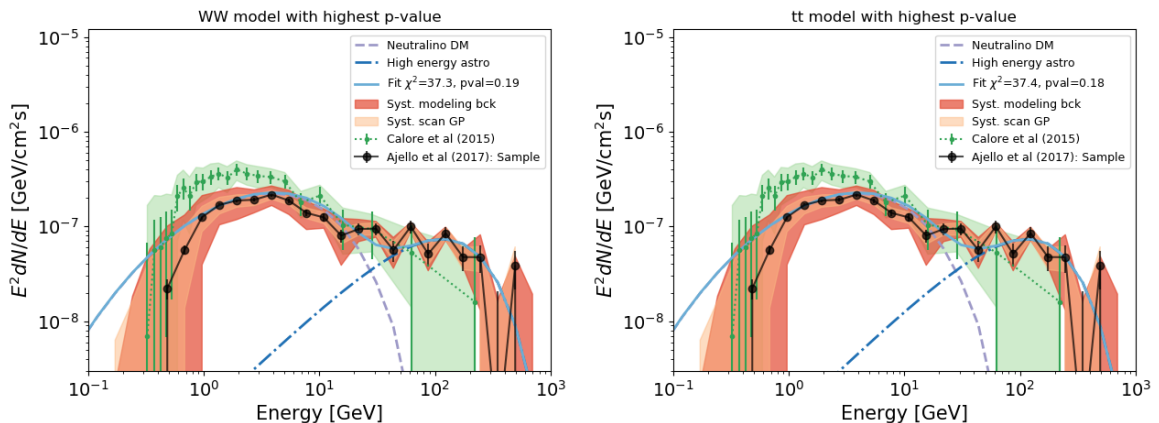


Figure 4: Spectral energy distribution of the 100% DM models with the highest p-value. The left and right panel correspond to $WW/t\bar{t}$ type of solutions.

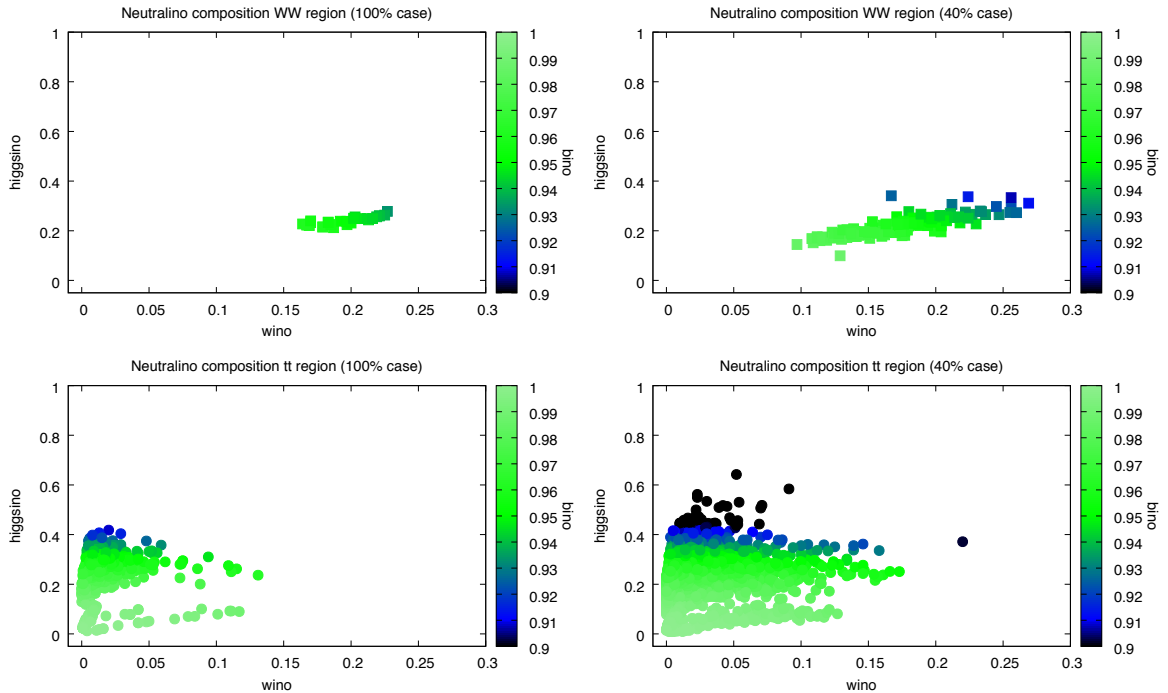
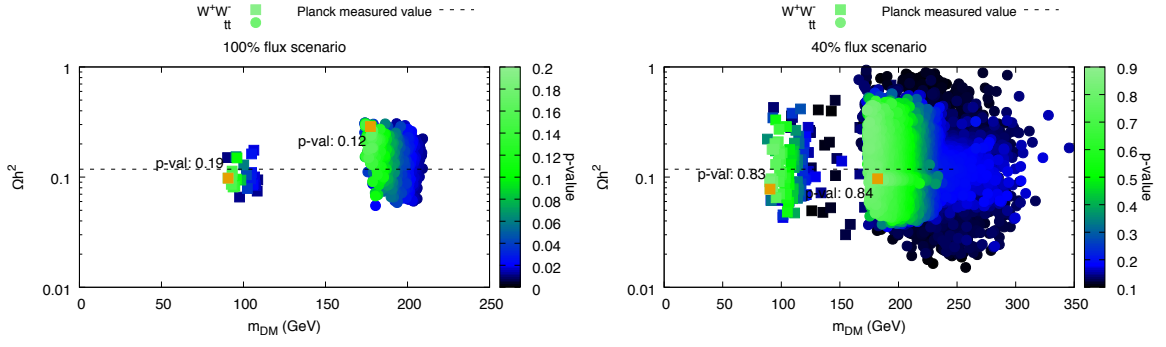


Figure 5: Composition of neutralino dark matter where $\text{bino} \equiv |N_{11}|$, $\text{wino} \equiv |N_{12}|$ and $\text{higgsino} \equiv (|N_{13}|^2 + |N_{14}|^2)^{1/2}$. Left and right panels represent the 100% and 40% flux scenarios respectively, while the top and bottom panels represent the WW/tt solutions.

Both dark matter solutions overlap with the solutions found in ref. [32] and ref. [33]. Figure 4 shows the spectrum of the GCE including the systematic uncertainties associated with the galactic diffuse emission modeling, as outlined in section 2, together with the spectra predicted by the pMSSM for the points giving the best p-value in the two regions identified in our scan. We will now discuss each of the regions separately.

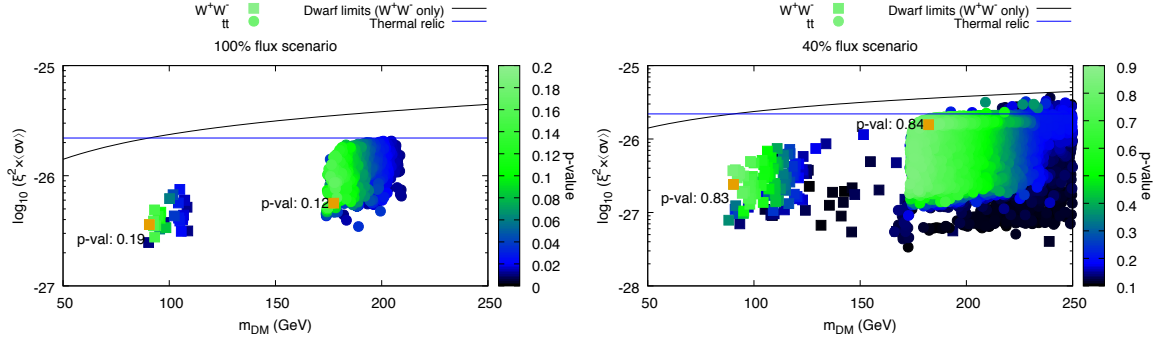
In the W^+W^- region, the dominant DM annihilation channel is mediated by a light chargino in the t-channel for present-day annihilation. If the predicted relic density does not make up the measured value of $\Omega h^2 = 0.118$ [87], the neutralino contributes only a fraction $\xi = \frac{\Omega h^2_{\text{model}}}{\Omega h^2_{\text{Planck}}}$ to the total Dark Matter. The photon flux from DM annihilation then needs to be rescaled by ξ^2 . The photon flux is proportional to the velocity-weighted present-day annihilation cross-section $\langle\sigma v\rangle$. To allow for a photon flux (and therefore $\xi^2\langle\sigma v\rangle$) that is big enough to explain the excess flux, we find that the DM particle must be bino-like with a smaller fraction of either wino, higgsino or both. Figure 5 shows the bino, wino and higgsino composition of the solutions. Larger wino and higgsino compositions yield a too efficient early universe annihilation and therefore rather small values of ξ that is too small to explain the GCE. A larger higgsino composition is also constrained by the limits on the spin-dependent DM-nucleus scattering cross section. Adding some wino fraction relaxes these direct detection constraints.

Figures 6a and 6b show the relic density of the obtained models. We are agnostic about the cosmological model that gives rise to the DM abundance we observe today, therefore we do not imply any constraints on Ωh^2 . The relic density of models that have a high p-value is around the measured value. This is remarkable since the MSSM has many regions



(a) Neutralino mass against Ωh^2 for the 100% scenario

(b) Neutralino mass against Ωh^2 for the 40% scenario

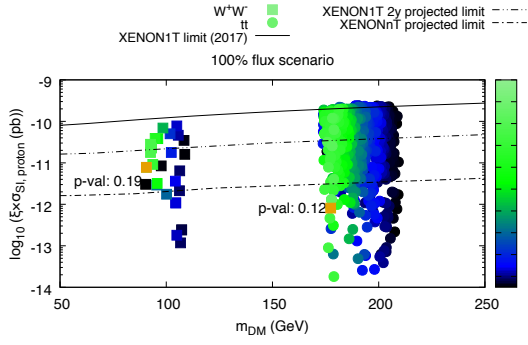


(c) Neutralino mass against $\xi^2 \langle \sigma v \rangle$ for the 100% scenario

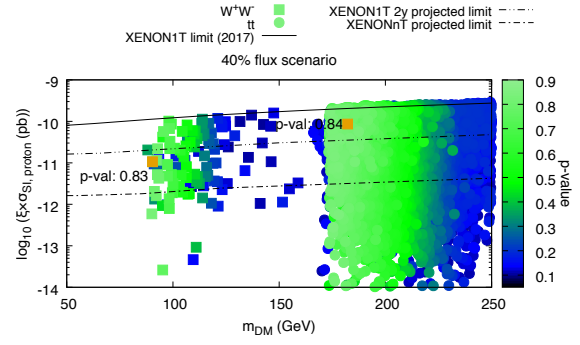
(d) Neutralino mass against $\xi^2 \langle \sigma v \rangle$ for the 40% scenario

Figure 6: Neutralino mass against Ωh^2 and $\langle \sigma v \rangle$. The cross section is rescaled with a factor $\xi^2 = (\Omega h^2_{\text{Model}} / \Omega h^2_{\text{Planck}})^2$ when Ωh^2 is smaller than the measured Planck value [88]. The left panel represents the 100% flux scenario while the right panel represents the 40% flux scenario.

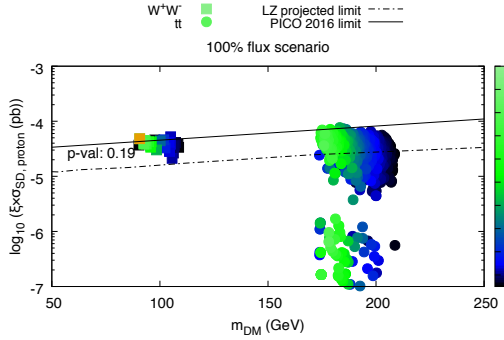
without a strong correlation between the relic density and the present-day DM annihilation cross section. For the same annihilation cross section, co-annihilation processes in the early Universe can result in vastly different relic densities.



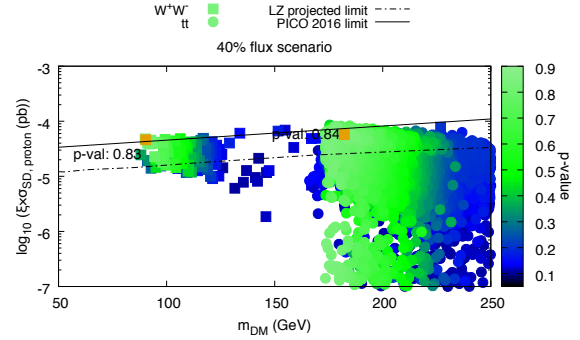
(a) Neutralino mass against $\xi\sigma_{\text{SI,proton}}$ for the 100% flux scenario



(b) Neutralino mass against $\xi\sigma_{\text{SI,proton}}$ for the 40% flux scenario



(c) Neutralino mass against $\xi\sigma_{\text{SD,proton}}$ for the 100% flux scenario



(d) Neutralino mass against $\xi\sigma_{\text{SD,proton}}$ for the 40% flux scenario

Figure 7: List of dark matter proton cross section plots. The cross sections are rescaled with a factor $\xi = \Omega h^2_{\text{Model}} / \Omega h^2_{\text{Planck}}$ when Ωh^2 is smaller than the measured Planck value [88]. The left panel represents the 100% flux scenario while the right panel represents the 40% flux scenario.

The values for $\xi^2 \langle \sigma v \rangle$ for the obtained models are shown in figures 6c and 6d. In contrast to simplified model DM explanations of the GCE, the photon flux is below the current *Fermi*-LAT limits from dwarf spheroidal galaxies [86] and $\xi^2 \langle \sigma v \rangle$ is below the thermal annihilation rate of $3 \times 10^{-26} \text{ cm}^3 \text{ s}^{-1}$.

In figures 7a and 7c the spin-independent (SI) and spin-dependent (SD) neutralino-proton cross-sections are shown. The projected and current sensitivities (90% CL exclusion limit) for the XENONnT, XENON1T, PICO and LZ experiments are also shown in these figures. We can observe that the complete W^+W^- region for the 100% flux scenario can be probed by the LZ experiment.

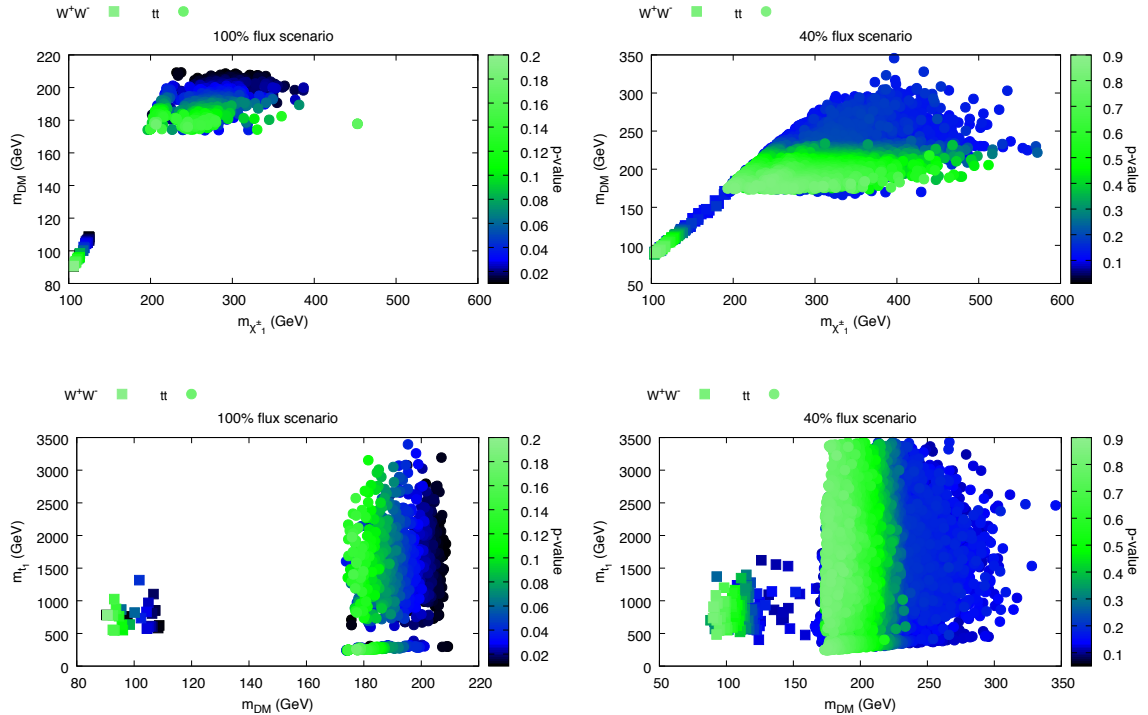


Figure 8: Top lane: DM vs lightest chargino mass (in GeV) for the 100% flux scenario (left) and the 40% flux scenario (right). Bottom lane: DM vs lightest stop mass (in GeV) for the 100% flux scenario (left) and the 40% flux scenario (right).

Finally, we turn our attention to LHC phenomenology. For the W^+W^- region, the only relevant masses are given in the electroweak SUSY sector (the charginos and the neutralinos). In figure 8 we show the mass of the co-annihilation partner (the chargino) vs the mass of the DM particle. For both the 100% and the 40% flux scenario, the lightest chargino $\tilde{\chi}_1^\pm$ and the next-to-lightest neutralino $\tilde{\chi}_2^0$ are close in mass with the DM particle. Their decays would create final state particles that are relatively low energetic. In addition the production cross section of a wino-bino or higgsino-bino $\tilde{\chi}_2^0$ in processes like $\tilde{\chi}_2^0\tilde{\chi}_1^\pm$ is reduced compared to the 100% wino $\tilde{\chi}_2^0$ and $\tilde{\chi}_1^\pm$ production scenarios studied in most LHC chargino-neutralino searches, such as in ref. [89, 90]. To probe these models, one would need a dedicated compressed search as proposed in ref. [40]. Another possibility is to search for signs of the heavier electroweak SUSY particles. For most models they are relatively light (< 500 GeV) and decay to $\tilde{\chi}_1^+W^-$ or $\tilde{\chi}_1^+Z$. These could therefore trigger a signal in the dilepton and/or in the trilepton plus missing transverse energy channel, but have a reduced cross section as compared to the lighter mass states.

In the $t\bar{t}$ region, the DM particle annihilates predominantly to pairs of top quarks. There are three kinds of mechanisms responsible for the annihilation into top quark pairs. For DM particles that are almost purely bino, the annihilation happens exclusively via the hypercharge enhanced right-handed stop t-channel. These models all have a low stop mass (figure 9, middle lane). A second region consists of DM particles that have a sizable higgsino component. These particles annihilate via the higgsino-pair annihilation channel via an s-

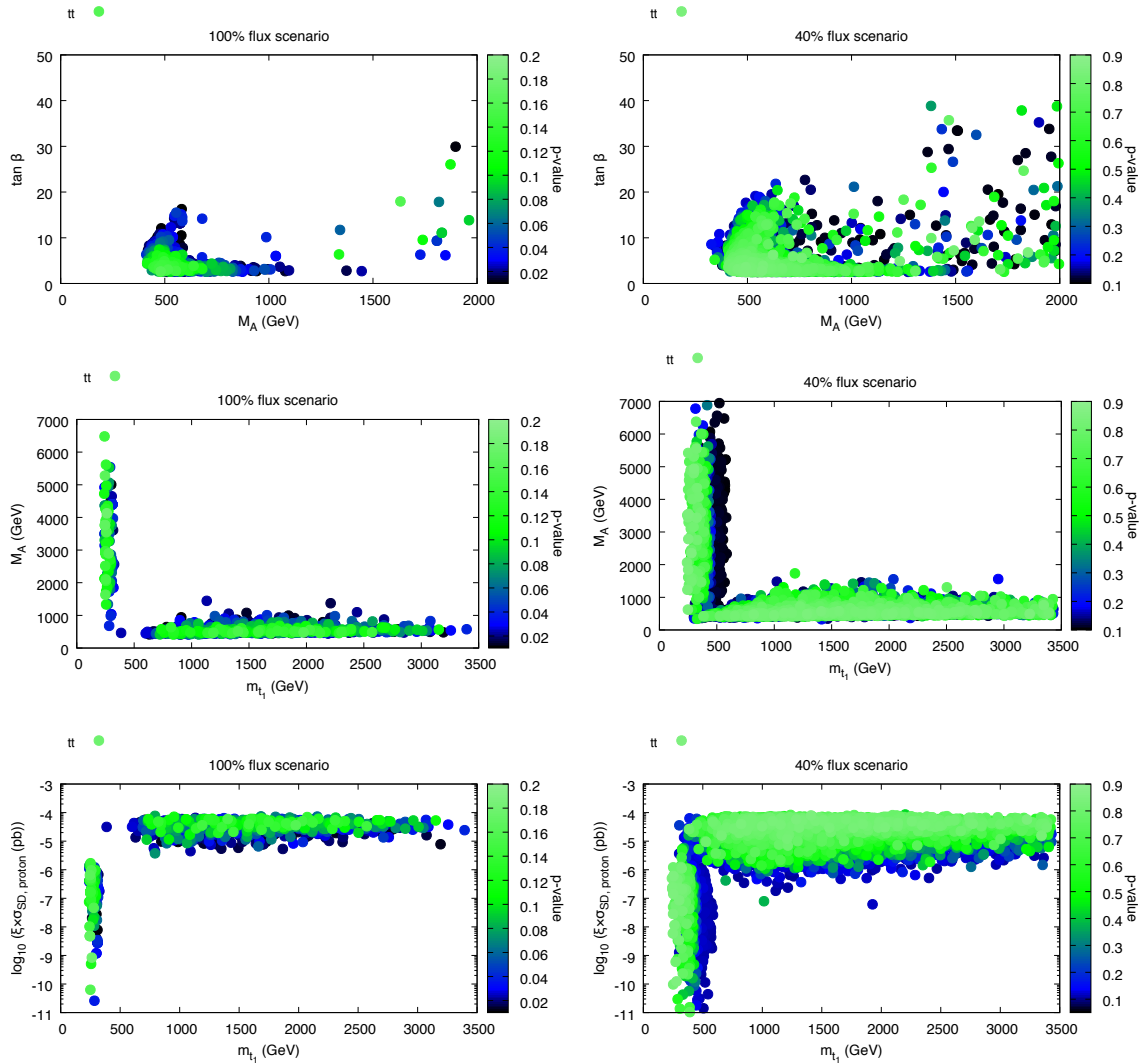


Figure 9: Top lane: M_A (in GeV) vs $\tan\beta$. Middle lane: Stop mass vs M_A (both in GeV). Bottom lane: spin-dependent dark matter proton scattering cross section vs the stop mass (in GeV). The 100% flux scenario is shown on the left side and the 40% flux scenario is shown on the right side. Only the $t\bar{t}$ solutions are shown.

channel Z -boson exchange¹¹. These contributions become relevant when the lightest stop mass is > 500 GeV, since then the t -channel is then suppressed. If the neutralino mass is around 250 GeV a third possibility arises, which was first discovered in ref. [35]. For these neutralino masses, tops are produced via an s -channel exchange of the CP-odd Higgs boson with a mass around 500 GeV. The two higgsino enhanced regions are characterized by a low $\tan\beta < 16$ and moderately low values for M_A . Regarding the relic abundance, we find points below the Planck bound as it can be seen in figure 6a and 6b that correspond to solutions in which the lightest stop is almost degenerate with the DM particle and therefore they co-annihilate efficiently. It is remarkable that the point with the best p -value in this

¹¹The annihilation to $t\bar{t}$ -pairs is enhanced due to the helicity suppression that occurs for the annihilation to lighter fermions.

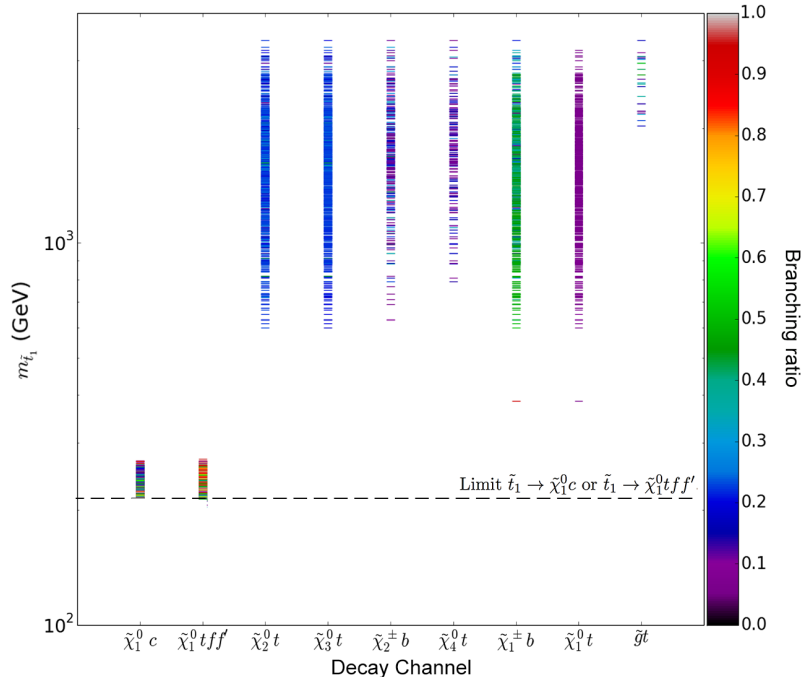


Figure 10: Decay spectrum for the $t\bar{t}$ solutions in the 100% flux scenario. The LHC limit for the decays $\tilde{t}_1 \rightarrow \tilde{\chi}_1^0 c$ and/or $\tilde{t}_1 \rightarrow \tilde{\chi}_1^0 t f f'$ [78] is indicated by the dashed line. For heavier stops the simplified limits are not applicable.

region has the correct relic abundance. The $t\bar{t}$ models are not in any tension with direct detection experiments. The models that have a very low $\sigma_{\text{SD},p}$ correspond to solutions where the neutralino is almost a pure bino and therefore the Z -boson coupling vanishes. This can also be seen in figure 9 (bottom lane), where $\sigma_{\text{SD},p}$ is plotted against the stop mass.

At the LHC the $t\bar{t}$ models can be probed via electroweak searches, searches for stop particles and searches for heavy Higgs bosons. Other SUSY particles are not relevant for the GCE interpretation. For some of the solutions, the lightest stop has a very low mass (< 500 GeV, see figure 8), thus it would be produced copiously at the LHC. The decays for the $t\bar{t}$ models are shown in figure 10, together with the branching fractions as a color code. Models where the stop decays exclusively to the lightest chargino and a b-jet are excluded by the LHC bounds [79]. If the chargino is heavier than the stop, the stop decays to three fermions and a neutralino or to a charm and a neutralino. In these cases LHC bounds are weaker and stops are only excluded if the stop mass is below 220 GeV [78]. The obtained solutions are not in tension with the limits on heavy Higgs bosons [91] or electroweak SUSY particles.

Additionally the electroweak fine-tuning of the allowed models was calculated using the procedure from ref. [41, 92, 93]. We find that the W^+W^- region has a low fine-tuning (< 20) overall, while the $t\bar{t}$ region has models which have a low fine-tuning as well. For our solutions, the higgsino component of the lightest neutralino essentially drives the value of the fine-tuning: the neutralinos with a higher higgsino component will result in models that have a lower fine-tuning. We therefore find that the W^+W^- region has low fine-tuning. The $t\bar{t}$ models that have a low stop mass result in a higher fine-tuning, since the higgsino component of the neutralino is very small. The $t\bar{t}$ region does possess models with low values for the fine-tuning for the higgsino enhanced region. Details on the fine-tuning calculation can be

found in ref. [41]. The fact that the models that can explain the GC excess also have a low fine-tuning is noteworthy.

5 Conclusion

In this analysis we verify that the phenomenological minimal supersymmetric standard model (pMSSM) can still explain the Galactic Center excess (GCE) using the Pass 8 data from *Fermi*-LAT and updated detector limits. We assume that dark matter annihilation is partially responsible for the excess flux between photon energies of 1 and 10 GeV. To account for the high energy tail of the excess, starting at photon energies of 10 GeV, a free power law was fitted. This resembles another astrophysical source to which we give no further interpretation. Within the minimal supersymmetric extension of the Standard Model, two types of dark matter solutions are found that can explain the GCE:

- **W^+W^- region:** A neutralino with a mass between 80 and 120 GeV with the dominant neutralino annihilation channel being W^+W^- . The composition of the neutralino is mainly bino, with a smaller fraction of either wino or higgsino.
- **$t\bar{t}$ region:** A neutralino with a mass between 175 and 220 GeV annihilating predominantly to $t\bar{t}$. This solution splits up into two regions. If the neutralino is almost purely bino, the stop mass is typically close to the neutralino mass leading to a compressed stop-neutralino spectrum. If the neutralino has an enhanced higgsino component, the stop particle can have a mass up to a few TeV. The latter region is characterized by a heavy Higgs boson mass between 500 GeV and 1 TeV.

It should be noted that in both regions, we find models that have a very low value for the electroweak fine-tuning. The direct dark matter detection experiments that provide limits on the spin-dependent dark matter-nucleus cross section will be able to probe the complete W^+W^- region in the near future. The higgsino enhanced $t\bar{t}$ region can also be probed by these direct detection experiments. The LHC is able to probe the $t\bar{t}$ region and the W^+W^- region via low mass stop searches, searches for heavy Higgs bosons and compressed chargino-neutralino searches.

Acknowledgements

This paper uses the GCE extracted from [16], we thank Dmitry Malyshev for making the data available here https://www-glast.stanford.edu/pub_data/1220/. We thank Johannes Buchner for his advice on the statistical method to deal with GCE spectra. R. RdA, is supported by the Ramón y Cajal program of the Spanish MICINN and also thanks the support of the Spanish MICINN's Consolider-Ingenio 2010 Programme under the grant MULTIDARK CSD2209-00064, the Invisibles European ITN project (FP7-PEOPLE-2011-ITN, PITN-GA-2011-289442-INVISIBLES, the "SOM Sabor y origen de la Materia" (FPA2011-29678), the "Fenomenologia y Cosmologia de la Fisica mas alla del Modelo Estandar e Implicaciones Experimentales en la era del LHC" (FPA2010-17747) MEC projects and the Spanish MINECO Centro de Excelencia Severo Ochoa del IFIC program under grant SEV-2014-0398. The work of GAGV was supported by Programa FONDECYT Postdoctorado under grant 3160153. SC and LH acknowledge the support within the "idark" program of the Netherlands eScience Center (NLeSC). M. van Beekveld acknowledges support by the Foundation for Fundamental Research of Matter (FOM), programme 156, "Higgs as Probe and Portal".

References

- [1] G. Bertone, D. Hooper, and J. Silk, "Particle dark matter: Evidence, candidates and constraints," *Phys. Rept.*, vol. 405, pp. 279–390, 2005.
- [2] W. B. Atwood, A. A. Abdo, M. Ackermann, W. Althouse, B. Anderson, M. Axelsson, L. Baldini, J. Ballet, D. L. Band, G. Barbiellini, and et al., "The Large Area Telescope on the Fermi Gamma-Ray Space Telescope Mission," *Astrophys. J.*, vol. 697, pp. 1071–1102, June 2009.
- [3] L. Goodenough and D. Hooper, "Possible Evidence For Dark Matter Annihilation In The Inner Milky Way From The Fermi Gamma Ray Space Telescope,"
- [4] V. Vitale and A. Morselli, "Indirect Search for Dark Matter from the center of the Milky Way with the Fermi-Large Area Telescope," in *Fermi gamma-ray space telescope. Proceedings, 2nd Fermi Symposium, Washington, USA, November 2-5, 2009*, 2009.
- [5] D. Hooper and L. Goodenough, "Dark Matter Annihilation in The Galactic Center As Seen by the Fermi Gamma Ray Space Telescope," *Phys. Lett. B*, vol. 697, pp. 412–428, 2011.
- [6] C. Gordon and O. Macias, "Dark Matter and Pulsar Model Constraints from Galactic Center Fermi-LAT Gamma Ray Observations," *Phys. Rev. D*, vol. 88, no. 8, p. 083521, 2013. [Erratum: *Phys. Rev. D*89,no.4,049901(2014)].
- [7] D. Hooper and T. Linden, "On The Origin Of The Gamma Rays From The Galactic Center," *Phys. Rev. D*, vol. 84, p. 123005, 2011.
- [8] T. Daylan, D. P. Finkbeiner, D. Hooper, T. Linden, S. K. N. Portillo, N. L. Rodd, and T. R. Slatyer, "The characterization of the gamma-ray signal from the central Milky Way: A case for annihilating dark matter," *Phys. Dark Univ.*, vol. 12, pp. 1–23, 2016.
- [9] A. Boyarsky, D. Malyshev, and O. Ruchayskiy, "A comment on the emission from the Galactic Center as seen by the Fermi telescope," *Phys. Lett. B*, vol. 705, pp. 165–169, Nov. 2011.
- [10] F. Calore, I. Cholis, and C. Weniger, "Background model systematics for the Fermi GeV excess," *JCAP*, vol. 1503, p. 038, 2015.
- [11] K. N. Abazajian, N. Canac, S. Horiuchi, and M. Kaplinghat, "Astrophysical and Dark Matter Interpretations of Extended Gamma-Ray Emission from the Galactic Center," *Phys. Rev. D*, vol. 90, no. 2, p. 023526, 2014.

- [12] B. Zhou, Y.-F. Liang, X. Huang, X. Li, Y.-Z. Fan, L. Feng, and J. Chang, “GeV excess in the Milky Way: The role of diffuse galactic gamma-ray emission templates,” *Phys. Rev. D*, vol. 91, no. 12, p. 123010, 2015.
- [13] J. F. Navarro, C. S. Frenk, and S. D. M. White, “A Universal Density Profile from Hierarchical Clustering,” *Astrophys. J.*, vol. 490, pp. 493–508, Dec. 1997.
- [14] J. F. Navarro, C. S. Frenk, and S. D. White, “The Structure of cold dark matter halos,” *Astrophys. J.*, vol. 462, pp. 563–575, 1996.
- [15] **Fermi/LAT** Collaboration, “Fermi-LAT Observations of High-Energy Gamma-Ray Emission toward the Galactic Center,” *Astrophys. J.*, vol. 819, p. 44, Mar. 2016.
- [16] M. Ackermann *et al.*, “The Fermi Galactic Center GeV Excess and Implications for Dark Matter,” *Astrophys. J.*, vol. 840, no. 1, p. 43, 2017.
- [17] J.-P. Macquart and N. Kanekar, “On Detecting Millisecond Pulsars at the Galactic Center,” *Astrophys. J.*, vol. 805, no. 2, p. 172, 2015.
- [18] A. McCann, “A stacked analysis of 115 pulsars observed by the Fermi LAT,” *Astrophys. J.*, vol. 804, no. 2, p. 86, 2015.
- [19] N. Mirabal, “Dark matter vs. Pulsars: Catching the impostor,” *Mon. Not. Roy. Astron. Soc.*, vol. 436, p. 2461, 2013.
- [20] R. M. O’Leary, M. D. Kistler, M. Kerr, and J. Dexter, “Young Pulsars and the Galactic Center GeV Gamma-ray Excess,” 2015.
- [21] Q. Yuan and B. Zhang, “Millisecond pulsar interpretation of the Galactic center gamma-ray excess,” *JHEAp*, vol. 3-4, pp. 1–8, 2014.
- [22] J. Petrovic, P. D. Serpico, and G. Zaharijas, “Millisecond pulsars and the Galactic Center gamma-ray excess: the importance of luminosity function and secondary emission,” *JCAP*, vol. 1502, p. 023, 2015.
- [23] I. Cholis, D. Hooper, and T. Linden, “Challenges in Explaining the Galactic Center Gamma-Ray Excess with Millisecond Pulsars,” *JCAP*, vol. 1506, p. 043, 2015.
- [24] S. K. Lee, M. Lisanti, B. R. Safdi, T. R. Slatyer, and W. Xue, “Evidence for Unresolved γ -Ray Point Sources in the Inner Galaxy,” *Phys. Rev. Lett.*, vol. 116, p. 051103, Feb. 2016.
- [25] R. Bartels, S. Krishnamurthy, and C. Weniger, “Strong Support for the Millisecond Pulsar Origin of the Galactic Center GeV Excess,” *Phys. Rev. Lett.*, vol. 116, p. 051102, Feb. 2016.
- [26] D. Hooper and G. Mohlabeng, “The Gamma-Ray Luminosity Function of Millisecond Pulsars and Implications for the GeV Excess,” *JCAP*, vol. 1603, p. 049, 2016.
- [27] D. Hooper and T. Linden, “The Gamma-Ray Pulsar Population of Globular Clusters: Implications for the GeV Excess,” *JCAP*, vol. 1608, p. 018, 2016.
- [28] D. Haggard, C. Heinke, D. Hooper, and T. Linden, “Low Mass X-Ray Binaries in the Inner Galaxy: Implications for Millisecond Pulsars and the GeV Excess,” *JCAP*, vol. 1705, p. 056, 2017.
- [29] H. Ploeg, C. Gordon, R. Crocker, and O. Macias, “Consistency Between the Luminosity Function of Resolved Millisecond Pulsars and the Galactic Center Excess,” *JCAP*, vol. 2017, p. 015, 2017.
- [30] S. Caron, G. A. G̃aszmez-Vargas, L. Hendriks, and R. Ruiz de Austri, “Analyzing gamma-rays of the Galactic Center with Deep Learning,” 2017.
- [31] A. Djouadi *et al.*, “The Minimal supersymmetric standard model: Group summary report,” in *GDR (Groupement De Recherche) - Supersymetrie Montpellier, France, April 15-17, 1998*, 1998.

- [32] A. Achterberg, S. Amoroso, S. Caron, L. Hendriks, R. Ruiz de Austri, and C. Weniger, “A description of the Galactic Center excess in the Minimal Supersymmetric Standard Model,” *JCAP*, vol. 1508, p. 006, 2015.
- [33] G. Bertone, F. Calore, S. Caron, R. Ruiz, J. S. Kim, R. Trotta, and C. Weniger, “Global analysis of the pMSSM in light of the Fermi GeV excess: prospects for the LHC Run-II and astroparticle experiments,” *JCAP*, vol. 1604, p. 037, 2016.
- [34] A. Butter, S. Murgia, T. Plehn, and T. M. P. Tait, “Saving the MSSM from the Galactic Center Excess,” *Phys. Rev. D*, vol. 96, no. 3, p. 035036, 2017.
- [35] K. Freese, A. Lopez, N. R. Shah, and B. Shakya, “MSSM A-funnel and the Galactic Center Excess: Prospects for the LHC and Direct Detection Experiments,” *JHEP*, vol. 1604, p. 059, 2016.
- [36] P. Agrawal, B. Batell, P. J. Fox, and R. Harnik, “WIMPs at the galactic center,” *JCAP*, vol. 1505, p. 011, 2015.
- [37] D. Cerdeno, M. Peiro, and S. Robles, “Fits to the Fermi-LAT GeV excess with RH sneutrino dark matter: implications for direct and indirect dark matter searches and the LHC,” *Phys. Rev. D*, vol. 91, no. 12, p. 123530.
- [38] J. Cao, L. Shang, P. Wu, J. M. Yang, and Y. Zhang, “Supersymmetry explanation of the Fermi Galactic Center excess and its test at LHC run II,” *Phys. Rev. D*, vol. 91, p. 055005, Mar. 2015.
- [39] M. Cahill-Rowley, J. Gainer, J. Hewett, and T. Rizzo, “Towards a Supersymmetric Description of the Fermi Galactic Center Excess,” *JHEP*, vol. 1502, p. 057, 2015.
- [40] M. van Beekveld, W. Beenakker, S. Caron, and R. Ruiz de Austri, “The case for 100 GeV bino dark matter: A dedicated LHC tri-lepton search,” *JHEP*, vol. 1604, p. 154, 2016.
- [41] M. van Beekveld, W. Beenakker, S. Caron, R. Peeters, and R. Ruiz de Austri, “Supersymmetry with Dark Matter is still natural,” *Phys. Rev. D*, vol. 96, no. 3, p. 035015, 2017.
- [42] D. S. Akerib *et al.*, “Results from a search for dark matter in the complete LUX exposure,” *Phys. Rev. Lett.*, vol. 118, no. 2, p. 021303, 2017.
- [43] A. Tan *et al.*, “Dark Matter Results from First 98.7 Days of Data from the PandaX-II Experiment,” *Phys. Rev. Lett.*, vol. 117, no. 12, p. 121303, 2016.
- [44] E. Aprile *et al.*, “First Dark Matter Search Results from the XENON1T Experiment,” 2017.
- [45] C. Amole *et al.*, “Dark Matter Search Results from the PICO-60 C₃F₈ Bubble Chamber,” *Phys. Rev. Lett.*, vol. 118, no. 25, p. 251301, 2017.
- [46] T. A. Porter, G. Johannesson, and I. V. Moskalenko, “High-Energy Gamma Rays from the Milky Way: Three-Dimensional Spatial Models for the Cosmic-Ray and Radiation Field Densities in the Interstellar Medium,” *Astrophys. J.*, vol. 846, no. 1, p. 67, 2017.
- [47] S. Horiuchi, M. Kaplinghat, and A. Kwa, “Investigating the Uniformity of the Excess Gamma rays towards the Galactic Center Region,” *JCAP*, vol. 1611, no. 11, p. 053, 2016.
- [48] T. Linden, N. L. Rodd, B. R. Safdi, and T. R. Slatyer, “High-energy tail of the Galactic Center gamma-ray excess,” *Phys. Rev.*, vol. D94, no. 10, p. 103013, 2016.
- [49] I. Moskalenko and A. Strong, “Production and propagation of cosmic ray positrons and electrons,” *Astrophys. J.*, vol. 493, pp. 694–707, 1998.
- [50] A. W. Strong, I. V. Moskalenko, and O. Reimer, “Diffuse continuum gamma-rays from the galaxy,” *Astrophys. J.*, vol. 537, pp. 763–784, 2000.
- [51] I. V. Moskalenko and A. W. Strong, “Anisotropic Inverse Compton Scattering in the Galaxy,” *Astrophys. J.*, vol. 528, pp. 357–367, Jan. 2000.

- [52] R. Andrae, T. Schulze-Hartung, and P. Melchior, “Dos and don’ts of reduced chi-squared,” *ArXiv e-prints*, Dec. 2010.
- [53] C. F. Berger, J. S. Gainer, J. L. Hewett, and T. G. Rizzo, “Supersymmetry Without Prejudice,” *JHEP*, vol. 0902, p. 023, 2009.
- [54] J. H. Kotecha and P. M. Djuric, “Gaussian particle filtering,” *IEEE Transactions on Signal Processing*, vol. 51, pp. 2592–2601, Oct 2003.
- [55] A. Djouadi, J.-L. Kneur, and G. Moultaka, “SuSpect: A Fortran code for the supersymmetric and Higgs particle spectrum in the MSSM,” *Comput. Phys. Commun.*, vol. 176, pp. 426–455, 2007.
- [56] H. Bahl and W. Hollik, “Precise prediction for the light MSSM Higgs boson mass combining effective field theory and fixed-order calculations,” *Eur. Phys. J. C*, vol. 76, no. 9, p. 499, 2016.
- [57] T. Hahn, S. Heinemeyer, W. Hollik, H. Rzehak, and G. Weiglein, “High-Precision Predictions for the Light CP -Even Higgs Boson Mass of the Minimal Supersymmetric Standard Model,” *Phys. Rev. Lett.*, vol. 112, no. 14, p. 141801, 2014.
- [58] M. Frank, T. Hahn, S. Heinemeyer, W. Hollik, H. Rzehak, and G. Weiglein, “The Higgs Boson Masses and Mixings of the Complex MSSM in the Feynman-Diagrammatic Approach,” *JHEP*, vol. 0702, p. 047, 2007.
- [59] G. Degrassi, S. Heinemeyer, W. Hollik, P. Slavich, and G. Weiglein, “Towards high precision predictions for the MSSM Higgs sector,” *Eur. Phys. J. C*, vol. 28, pp. 133–143, 2003.
- [60] S. Heinemeyer, W. Hollik, and G. Weiglein, “FeynHiggs: A Program for the calculation of the masses of the neutral CP even Higgs bosons in the MSSM,” *Comput. Phys. Commun.*, vol. 124, pp. 76–89, 2000.
- [61] D. Barducci, G. Belanger, J. Bernon, F. Boudjema, J. Da Silva, S. Kraml, U. Laa, and A. Pukhov, “Collider limits on new physics within micrOMEGAs,”
- [62] P. Gondolo, J. Edsjö, P. Ullio, L. Bergström, M. Schelke, E. Baltz, T. Bringmann, and G. Duda. <http://www.darksusy.org>.
- [63] “Lep2 susy working group, aleph, delphi, l3 and opal experiments, note lepsusywg/01-03.1.”
- [64] M. Carena, A. de Gouvea, A. Freitas, and M. Schmitt, “Invisible Z boson decays at e+ e- colliders,” *Phys. Rev. D*, vol. 68, p. 113007, 2003.
- [65] G. Aad *et al.*, “Measurement of the Higgs boson mass from the $H \rightarrow \gamma\gamma$ and $H \rightarrow ZZ^* \rightarrow 4\ell$ channels with the ATLAS detector using 25 fb⁻¹ of pp collision data,” *Phys. Rev. D*, vol. 90, p. 052004, 2014.
- [66] B. L. Roberts, “Status of the Fermilab Muon ($g - 2$) Experiment,” *Chin. Phys.*, vol. C34, pp. 741–744, 2010.
- [67] R. Aaij *et al.*, “Measurement of the $B_s^0 \rightarrow \mu^+ \mu^-$ branching fraction and search for $B^0 \rightarrow \mu^+ \mu^-$ decays at the LHCb experiment,” *Phys. Rev. Lett.*, vol. 111, p. 101805, 2013.
- [68] M. Misiak *et al.*, “Updated NNLO QCD predictions for the weak radiative B-meson decays,” *Phys. Rev. Lett.*, vol. 114, no. 22, p. 221801, 2015.
- [69] M. Czakon, P. Fiedler, T. Huber, M. Misiak, T. Schutzmeier, and M. Steinhauser, “The $(Q_7, Q_{1,2})$ contribution to $\bar{B} \rightarrow X_s \gamma$ at $\mathcal{O}(\alpha_s^2)$,” *JHEP*, vol. 1504, p. 168, 2015.
- [70] B. Kronenbitter *et al.*, “Measurement of the branching fraction of $B^+ \rightarrow \tau^+ \nu_\tau$ decays with the semileptonic tagging method,” *Phys. Rev. D*, vol. 92, no. 5, p. 051102, 2015.
- [71] L. Widhalm *et al.*, “Measurement of $B(D(s)^+ \rightarrow \mu(\nu))$,” *Phys. Rev. Lett.*, vol. 100, p. 241801, 2008.

- [72] P. U. E. Onyisi *et al.*, “Improved Measurement of Absolute Branching Fraction of $D(s)^+ \rightarrow \tau^+ \nu_\tau$,” *Phys. Rev. D*, vol. 79, p. 052002, 2009.
- [73] P. Bechtle, S. Heinemeyer, O. Stal, T. Stefaniak, and G. Weiglein, “Applying Exclusion Likelihoods from LHC Searches to Extended Higgs Sectors,” *Eur. Phys. J. C*, vol. 75, no. 9, p. 421, 2015.
- [74] S. Caron, J. S. Kim, K. Rolbiecki, R. Ruiz de Austri, and B. Stienen, “The BSM-AI project: SUSY-AI—generalizing LHC limits on supersymmetry with machine learning,” *Eur. Phys. J. C*, vol. 77, no. 4, p. 257, 2017.
- [75] A. Barr and J. Liu, “Analysing parameter space correlations of recent 13 TeV gluino and squark searches in the pMSSM,” *Eur. Phys. J. C*, vol. 77, no. 3, p. 202, 2017.
- [76] **ATLAS** Collaboration, “Search for direct top squark pair production and dark matter production in final states with two leptons in $\sqrt{s} = 13$ TeV pp collisions using 13.3 fb $^{-1}$ of ATLAS data,” 2016.
- [77] **ATLAS** collaboration, “Search for new phenomena in final states with an energetic jet and large missing transverse momentum in pp collisions at $\sqrt{s} = 13$ TeV using the ATLAS detector,” *Phys. Rev. D*, vol. 94, no. 3, p. 032005, 2016.
- [78] **ATLAS** collaboration, “Search for pair-produced third-generation squarks decaying via charm quarks or in compressed supersymmetric scenarios in pp collisions at $\sqrt{s} = 8$ TeV with the ATLAS detector,” *Phys. Rev. D*, vol. 90, no. 5, p. 052008, 2014.
- [79] **CMS** collaboration, “Search for direct production of supersymmetric partners of the top quark in the all-jets final state in proton-proton collisions at $\sqrt{s} = 13$ TeV,” 2017.
- [80] T. Bringmann *et al.*, “DarkBit: A GAMBIT module for computing dark matter observables and likelihoods,” 2017.
- [81] **ATLAS** collaboration, “Summary of the ATLAS experiment’s sensitivity to supersymmetry after LHC Run 1 interpreted in the phenomenological MSSM,” *JHEP*, vol. 1510, p. 134, 2015.
- [82] M. G. Aartsen *et al.*, “Search for annihilating dark matter in the Sun with 3 years of IceCube data,” *Eur. Phys. J. C*, vol. 77, no. 3, p. 146, 2017.
- [83] F. Calore, I. Cholis, C. McCabe, and C. Weniger, “A Tale of Tails: Dark Matter Interpretations of the Fermi GeV Excess in Light of Background Model Systematics,” *Phys. Rev. D*, vol. 91, no. 6, p. 063003, 2015.
- [84] J. Albert *et al.*, “Observation of gamma-rays from the galactic center with the magic telescope,” *Astrophys. J.*, vol. 638, pp. L101–L104, 2006.
- [85] M. Ackermann *et al.*, “Searching for Dark Matter Annihilation from Milky Way Dwarf Spheroidal Galaxies with Six Years of Fermi Large Area Telescope Data,” *Phys. Rev. Lett.*, vol. 115, no. 23, p. 231301, 2015.
- [86] M. L. Ahnen *et al.*, “Limits to dark matter annihilation cross-section from a combined analysis of MAGIC and Fermi-LAT observations of dwarf satellite galaxies,” *JCAP*, vol. 1602, no. 02, p. 039, 2016.
- [87] **Planck** Collaboration, P. Ade *et al.*, “Planck 2013 results. XVI. Cosmological parameters,” *Astron. Astrophys.*, vol. 571, p. A16, 2014.
- [88] E. Aprile *et al.*, “Physics reach of the XENON1T dark matter experiment,” *JCAP*, vol. 1604, no. 04, p. 027, 2016.
- [89] **CMS** collaboration, “Search for new physics in events with two low momentum opposite-sign leptons and missing transverse energy at $\sqrt{s} = 13$ TeV,” no. CMS-PAS-SUS-16-048, 2017.
- [90] **ATLAS** collaboration, “Search for electroweak production of supersymmetric particles in the two and three lepton final state at $\sqrt{s} = 13$ TeV with the ATLAS detector,” Jun 2017.

- [91] **ATLAS** collaboration, “Search for heavy Higgs bosons A/H decaying to a top quark pair in pp collisions at $\sqrt{s} = 8$ TeV with the ATLAS detector,” 2017.
- [92] H. Baer, V. Barger, P. Huang, A. Mustafayev, and X. Tata, “Radiative natural supersymmetry with a 125 gev higgs boson,” *Phys. Rev. Lett.*, vol. 109, p. 161802, Oct 2012.
- [93] H. Baer, V. Barger, P. Huang, D. Mickelson, A. Mustafayev, and X. Tata, “Radiative natural supersymmetry: Reconciling electroweak fine-tuning and the higgs boson mass,” *Phys. Rev.*, vol. D87, p. 115028, Jun 2013.